Carbohydrate Polymers 95 (2013) 91–99

Contents lists available at SciVerse ScienceDirect

Carbohydrate Polymers

journal homepage: www.elsevier.com/locate/carbpol

# Structure and mechanical properties of new biomass-based nanocomposite: Castor oil-based polyurethane reinforced with acetylated cellulose nanocrystal

Song Lin[a], Jin Huang[a,*], Peter R. Chang[b], Siwen Wei[c], Yixiang Xu[d], Qiaoxin Zhang[c]

[a] College of Chemical Engineering, Wuhan University of Technology, Wuhan 430070, China
[b] BioProducts and Bioprocesses National Science Program, Agriculture and Agri-Food Canada, Saskatoon, SK S7N 0X2, Canada
[c] School of Materials Science and Engineering, Wuhan University of Technology, Wuhan 430070, China
[d] School of Chemical Engineering and Pharmacy, Wuhan Institute of Technology, Wuhan 430073, China

ARTICLE INFO

*Article history:*
Received 11 September 2012
Received in revised form
30 December 2012
Accepted 11 February 2013
Available online 5 March 2013

*Keywords:*
Polyurethane
Cellulose nanocrystals
Acetylation
Nanocomposites
Mechanical properties
Percolating network

ABSTRACT

New nanocomposites consisting of a castor oil-based polyurethane matrix filled with acetylated cellulose nanocrystals (ACNs) were developed. The ACN exhibited improved dispersion in tetrahydrofuran as a blending medium, and reduced polarity as compared with unmodified cellulose nanocrystals, resulting in a high loading level of 25 wt% in the nanocomposite. As the ACN loading-level increased from 0% to 25%, the tensile strength and Young's modulus of the nanocomposites increased from 2.79 MPa to 10.41 MPa and from 0.98 MPa to 42.61 MPa, respectively. When the ACN loading-level was 10 wt%, the breaking elongation of the nanocomposites reached the maximum value of more than twice that of the polyurethane. The enhanced mechanical performance was primarily attributed to the formation of a three-dimensional ACN network and strong interfacial interactions between filler and matrix. This work produced new polyurethane-based nanocomposites containing modified cellulose nanocrystal with a high biomass content. Its high performance could contribute to potential applications.

## 1. Introduction

Over the past two decades, investigation and development of polymer nanocomposites have attracted great attention (Hussain, Hojjati, Okamoto, & Gorga, 2006). Most excitingly, a significant improvement in mechanical properties has been observed when high aspect ratio nanoscale filler (such as silica, clay and carbon nanotubes) are incorporated into neat polymer or composite systems (Tjong, 2006). Recently, cellulose nanocrystals have attracted interest because they are abundant and renewable, and have outstanding mechanical properties (Dufresne, 2008; Habibi, Lucia, & Rojas, 2010). The rod-like nanoparticles can be isolated from a variety of renewable sources including wood, cotton, straw, bacteria, and sea animals called tunicates (Lin, Chen, Huang, Dufresne, & Chang, 2009). Nanoparticles generally display a high surface area, unique morphology, low density, and good mechanical strength. About 17 years ago, Favier, Chanzy, and Cavaillé (1995) reported on the use of cellulose nanocrystals as reinforcing fillers in poly(styrene-co-butyl acrylate) (poly(Sco-BuA))-based nanocomposites. The powerful mechanical enhancement observed in these materials was explained by the formation of a percolating particle network in the polymer matrix, in which stress transfer among the particles was facilitated by hydrogen-bonding. Since then, there is an extensive list of nanocomposites comprising cellulose nanocrystals and modified cellulose nanocrystals in matrices such as poly(ethylene oxide) (Azizi Samir, Alloin, Sanchez, Dufresne, 2004; Azizi Samir, Alloin, Sanchez, El Kissi, Dufresne, 2004), poly(vinyl chloride) (Chazeau, Cavaillé, Canova, Dendievel, & Boutherin, 1999), poly(β-hydroxyoctanoate) (Dubief, Samain, & Dufresne, 1999), starch (Anglès & Dufresne, 2000), polypropylene (Ljungberg et al., 2005), poly(caprolactone) (Morin & Dufresne, 2002), ethylene oxide/epichlorohydrin copolymers (Capadona, Shanmuganathan, Tyler, Rowan, & Weder, 2008; Schroers, Kokil, & Weder, 2004), polystyrene (Capadona et al., 2007), polybutadiene (Capadona et al., 2007), poly(vinyl alcohol) (Shanmuganathan, Capadona, Rowan, & Weder, 2010a, 2010b), poly(butyl methacrylate) (Shanmuganathan et al., 2010a, 2010b), and polyurethanes (Cao, Dong, & Li, 2007; Wu, Henriksson, Liu, & Berglund, 2007) that have been explored. Aside from the previously stated matrices, Capadona et al. (2008) reported a unique nanocomposite

---

[*] Corresponding author at: College of Chemical Engineering, Wuhan University of Technology, 122 Loushi Road, Wuhan 430070, China. Tel.: +86 27 63373510; fax: +86 27 87859019.

*E-mail address:* huangjin@iccas.ac.cn (J. Huang).

0144-8617/$ – see front matter. Crown Copyright © 2013 Published by Elsevier Ltd. All rights reserved.
http://dx.doi.org/10.1016/j.carbpol.2013.02.023

based on a rubbery host polymer and rigid cellulose nanofibers that mimic sea cucumbers which have the ability to rapidly and reversibly alter stiffness. In addition, Shopsowitz, Qi, Hamad, and MacLachlan (2010) reported recently on cellulose nanocrystals that self-assembled in the matrix to form a chiral nematic phase with a structure that was similar to that of iridescent beetle exoskeletons.

The key factor affecting the mechanical enhancement of cellulose nanocrystals in the composite is their homogeneous dispersion in the polymeric matrix. However, due to the high surface area and hydrophilic nature of nanocrystals, intermolecular hydrogen bonding cause self-aggregation of nanocrystals, and hence give inefficient compounding with most nonpolar thermoplastics. Cao et al. incorporated cellulose nanocrystals into waterborne polyurethane to prepare thermoplastic nanocomposites and induced the formation of a co-continuous phase between the matrix and filler which significantly enhanced the interfacial adhesion. Consequently, this contributed to an improvement in the thermal stability and mechanical strength of the nanocomposites (Cao, Habibi, & Lucia, 2009). Gao et al. (2012) reported that cellulose nanocrystals with low loading levels showed good dispersion in a waterborne polyurethane matrix and significantly enhanced the tensile strength and Young's modulus. Incorporation of 1 wt% cellulose nanocrystals led to a 8-fold increase in tensile strength and 1.3-fold increase in strain-to-failure as reported by Zhou et al. (Pei, Malho, Ruokolainen, Zhou, & Berglund, 2011). However, all these improvements were either realized using lower volume fractions of biomass or were limited by the dispersibility of CN in polar solvents due to the surface hydroxyl groups of CN.

According to our previous work (Lin, Huang, Chang, Feng, & Yu, 2011), the surface of cellulose nanocrystals was chemically modified by acetic anhydride to provide acetylated cellulose nanocrystals (ACNs). With the substitution of hydroxyl groups on the CN surface by acetyl groups, acetylated cellulose nanocrystals exhibited improved dispersion in organic solvents, such as THF. In this work, we introduced acetylated cellulose nanocrystals into the castor oil based polyurethane formulation to stiffen and strengthen the material at very high biomass loading levels. Subsequently, the structure and mechanical properties of CN, ACN and the resultant nanocomposite materials were investigated by solid state $^{13}$C cross polarization-magic angle spinning nuclear magnetic resonance spectra ($^{13}$C CP-MAS NMR), Fourier transform infrared (FTIR) spectroscopy, X-ray diffraction (XRD), differential scanning calorimetry (DSC), dynamic mechanical analysis (DMA), scanning electron microscopy (SEM), transmission electron microscopy (TEM) and tensile tests.

## 2. Experimental

### 2.1. Materials

All chemical reagents were of analytical grade and obtained from commercial sources in China. 2,4-Toluene diisocyanate (TDI) was redistilled before use. Castor oil was further dehydrated at 100 °C under 20 mm Hg for 1 h. The linter was kindly supplied by Hubei Chemical Fiber Group Co., Ltd. (Xiangfan, Hubei, China).

### 2.2. Extraction and acetylation of cellulose nanocrystal

Cellulose nanocrystals (CNs) were prepared by acid hydrolysis of native linter using the following method: The linter (20.0 g) was dispersed in 175 mL of 30% (v/v) aqueous $H_2SO_4$ and stirred constantly at 100 rpm for 6 h at 60 °C. The resultant suspension was washed by continuous centrifugation with distilled water, and then a small amount of ammonia (0.5 wt%) was added to react with the sulfate groups from the CN surface to achieve approximate neutrality. The suspension was then dialyzed overnight against distilled water, and finally a loose powder was obtained by freeze-drying the CN. Acetylated cellulose nanocrystals were prepared according to the procedure described in the literature (Lin et al., 2011), and the detailed process was depicted as follows. Acetylation reaction was performed with constant stirring under a nitrogen atmosphere in a three-necked round-bottomed flask equipped with a condenser. Firstly, a suspension of 1.0 g cellulose nanocrystals and 20 mL anhydrous pyridine was dispersed by 15 min of ultrasonic treatment and then added to the flask. Subsequently, acetylation modification started by dropwise adding a solution of 5 mL acetic anhydride in a hydrous pyridine into the CN suspension. The reaction mixture was kept at 80 °C and stirred at 400 rpm for 5 h. After the reaction stopped, the product was precipitated in 1.0 L of water, and then washed three times with water. At last, the acetylated CN (ACN) was purified by washing with a solution of acetone/water to remove unreacted compounds and by-products.

### 2.3. Preparation of PU/ACN nanocomposites

The castor oil-based PU prepolymer (NCO/OH = 2) was prepared according to the method described by Sperling (Sperling & Manson, 1983). PU prepolymer (5 g) was mixed with the desired mass of ACN and 1,4-butanediol as the chain extender (the amount being adjusted to give total NCO/OH = 1) in THF at room temperature. The solids content of the resulting reactant solution was controlled at about 30 wt%, and then poured into a mold. The casting solutions were cured at room temperature for two days to form dried films that were about 0.5 mm thick. The PU/ACN films were coded as PU/ACN-5, PU/ACN-10, PU/ACN-15, PU/ACN-20 and PU/ACN/25, corresponding to the ACN content in the films of 5, 10, 15, 20 and 25 wt%, respectively. A neat PU film was also prepared according to the aforementioned process without the addition of ACN, and was coded as PU/ACN-0.

### 2.4. Characterization

FTIR spectra of the powdered CN and ACN, as well as all the nanocomposite films, were recorded on a 5700 FTIR spectrometer (Thermo Fisher, Madison, WI). The powders were scanned using a KBr-pellet method in the range of 4000–400 $cm^{-1}$ and the nanocomposite films were measured in the range of 4000–700 $cm^{-1}$.

X-ray diffraction measurements were performed on dry powders of CN and ACN, as well as on all nanocomposite films, at ambient temperature on a D/Max-IIIA X-ray diffractometer (Rigaku Denki, Tokyo, Japan) using Cu Kα radiation ($\lambda$ = 0.154 nm) at 40 kV and 60 mA. The diffraction angle of $2\theta$ ranged from 3° to 70°.

Solid state $^{13}$C cross polarization-magic angle spinning (CP-MAS) NMR spectra of CN and ACN were recorded at ambient temperature on a Varian Infinity-Plus 300 NMR spectrometer, using a MAS rate of 6 kHz, at a frequency of 75.5 MHz for $^{13}$C NMR. Samples were packed in 4-mm-diameter zirconia MAS rotors. All spectra were run for 3 h (3000 scans).

Contact angle measurements were carried out using a DSA10 dynamic drop tensiometer (KRÜSS, Germany) at room temperature. The contact angle and drop volume were monitored as a function of time using WINDROP software. Three different liquids with different dispersive and polar surface tensions were used to determine the surface energy of CN and ACN. The drop volume was ca. 5 μL. The powdered CN and ACN were each compacted under a pressure of 20 MPa with a KBr press to obtain samples with smooth surfaces.

The Owens–Wendt approach (Owens & Wendt, 1969) was used to relate the dispersive and polar contributions of the surface energies of the cellulose nanocrystal samples to those contributions of the surface tension of the liquids that were used. It was also used to relate the equilibrium contact angle with the cellulose nanocrystal surface (where the work of adhesion is replaced by the Young equation):

$$\gamma_L(1+\cos\theta) = 2\sqrt{\gamma_L^d\gamma_S^d} + 2\sqrt{\gamma_L^p\gamma_S^p} \tag{1}$$

The variables $\gamma$, $\gamma^d$ and $\gamma^p$ represent the total, dispersive, and polar surface energies, respectively. Subscripts "$L$" and "$S$" refer to the liquid drop ($L$) and the solid surface ($S$), and $\theta$ denotes the contact angle between the solid substrate and the liquid drop. The liquid surface tensions were taken from the literature (Lin et al., 2011; Ly EhB et al., 2010) and are listed in Table 1.

TEM photographs for the CN and the ultra-thin sections of PU/ACN-10 nanocomposite film were taken with an H-7000 FA transmission electron microscope (Hitachi, Japan) at 75 kV. TEM observations of ACN were carried out on a Tecnai transmission electron microscope (FEI Company, USA) at 200 kV. Small amounts of CN and ACN powders were dispersed separately in distilled water and then negatively stained with a 2% (w/v) ethanol solution of uranyl acetate. The ultra-thin sections of the PU/ACN-10 were obtained by embedding a piece of the sample in an epoxy resin block and then microtoming thin sections using a diamond knife.

The tensile strength ($\sigma_b$), elongation at break ($\varepsilon_b$) and Young's modulus ($E$) were measured on a CMT6503 universal testing machine (SANS, Shenzhen, China) with a crosshead rate of 100 mm min$^{-1}$ according to Test Method GB13022-91. The testing films were cut into strips 10 mm wide with a distance of 30 mm between testing marks. The testing strips were kept at 30% humidity for 7 days before measurement. An average value of five replicates of each sample was taken.

DSC experiments (Diamond DSC, PerkinElmer, MA, USA) were conducted in a nitrogen atmosphere at a heating or cooling rate of 20 °C min$^{-1}$. All nanocomposites were scanned over a range of −60 to 200 °C after a pretreatment of heating from 20 to 100 °C and then cooling to −60 °C to eliminate thermal history.

Dynamic mechanical analysis was performed using a DMA-242C dynamic mechanical analyzer (Netzsch, Germany) at a frequency of 1 Hz. Measurements were carried out over the range of −150 to 100 °C at a heating rate of 3 °C min$^{-1}$. A dual cantilever device was used and the dimensions of the test specimens (with a thickness of ca. 0.50 mm) were 15 mm × 5 mm.

SEM observations were carried out on a VEGA3 scanning electron microscope (TESCAN, Brno, Czech Republic) with an accelerating voltage of 25 kV. All nanocomposite films were frozen in liquid nitrogen and then immediately snapped. The fracture surfaces of the films were sputtered with gold and then observed and photographed.

## 3. Results and discussion

### 3.1. Structure and properties of acetylated cellulose nanocrystals

Using FTIR spectroscopy, successful reaction was characterized by the appearance of a new peak in the carbonyl area around 1745 cm$^{-1}$ that was associated with the formed ester group, shown in Fig. 1A. A new absorption band at 1240 cm$^{-1}$ was assigned to the carbonyl C—O stretch vibration. Acetylated cellulose nanocrystals were further characterized by $^{13}$C CP-MAS NMR spectroscopy (Fig. 1B). As in a previous report (Attala, Gast, Sindorf, Bartuska, & Maciel, 1980), carbons of the original CN were assigned as C1 (105 ppm), C4 crystalline (89 ppm), C4 amorphous (84 ppm), C2/C3/C5 (72 and 75 ppm), C6 crystalline (65 ppm), and C6 amorphous (63 ppm). After acetylation, there were two chemical shifts located at 172 and 20 ppm assigned, respectively, to Ca (—CO) and Cb (—CH$_3$) (shown in Fig. 1B) of the acetyl group on ACN, which confirmed the successful modification of CN.

The morphological changes associated with surface acetylation of cellulose nanocrystals were investigated by TEM. The original CN had a rodlike morphology with a length of 150–300 nm and a diameter of 10–25 nm, as shown in the TEM image in Fig. 1C, which was retained after acetylation. The impact of chemical modification on the crystallite structure of the cellulose nanocrystals was further investigated using XRD analysis. The diffraction patterns for unmodified CN and ACN are presented in Fig. 1D. Both two showed the typical reflection planes of cellulose I, i.e. 002, 101, and 040 for the diffraction peaks of the 2$\theta$ angles located at about 22.6°, 16.4°, and 34.4° (Liu, Liu, Yao, & Wu, 2010), respectively. It indicated that the original inner crystalline structure of the nanocrystals was maintained. The crystallinity index of unmodified CN and ACN were evaluated using the Buschle-Diller and Zeronian equation (Buschle-Diller & Zeronian, 1992):

$$I_c = 1 - \frac{I_1}{I_2} \tag{2}$$

where $I_1$ is the intensity at the minimum ($2\theta = 17.84°$) and $I_2$ is the intensity associated with the crystalline region of cellulose ($2\theta = 22.6°$). The results showed that the crystallinity index of CN and ACN were 88.1% and 74.2%, respectively. This further suggested the crystalline structure of the cellulose nanocrystals remained mostly intact.

Transformation of the surface characteristics of CN and ACN were further confirmed by the results of the contact angle measurements. Table 1 summarizes the equilibrium contact angles for water, diiodomethane and glycol on CN and ACN. The —OH covered CN surface was more capable of attaching to water and consequently had a lower initial contact angle value, which was consistent with reported literature (Fabbri, Champon, Castellano, Belgacem, & Gandini, 2004; Lin et al., 2011). The ACN had a sharp increase in $\theta_{\text{water}}$ from 36.3° to 60.7°, and a decrease in $\theta_{\text{diiodomethane}}$ from 32° to 30.0°, which indicated that chemical modification had induced dramatic changes in surface polarity of the cellulose nanocrystals. These observations were determined according to the Owens–Wendt approach by the values of the polar and dispersive contributions to the surface energy, as given in Table 1. With the introduction of nonpolar groups onto the surface of CN, the polar component decreased considerably, whereas the dispersive one evidently did not change. The polar component ($\gamma_s^p$) of the cellulose nanocrystals decreased from 29.5 to 12.7 mJ m$^{-2}$ while the total surface energy ($\gamma_s$) decreased from 63.1 to 50.6 mJ m$^{-2}$. This can be attributed to the substitution of hydrophilic —OH by acetyl groups. It should be pointed out that acetylated cellulose nanocrystals showed improved dispersion in organic solvent, such as the tetrahydrofuran (THF) blending media. Fig. 1E shows the dispersion photographs of CN and ACN in THF, and most CN in THF obviously precipitated pointed out by the arrow while almost no precipitate was observed for the ACN in THF. It indicated that acetylated cellulose nanocrystals existed in an organic matrix, such as PU, more homogeneously and with more stability than the unacetylated nanocrystals.

### 3.2. Mechanical properties of PU/ACN nanocomposites

Acetylated cellulose nanocrystals were incorporated into a PU matrix. Fig. 2 shows the effects of ACN content on the mechanical parameters of PU/ACN nanocomposites including tensile strength ($\sigma_b$), elongation at break ($\varepsilon_b$), and Young's modulus ($E$). The $E$ and $\sigma_b$ of the nanocomposites increased gradually with an increase in the ACN content. PU/ACN-25 had the highest loading level and the maximum $E$ and $\sigma_b$ values, 42.61 MPa and 10.41 MPa, respectively, which were about 44-fold and 3.7-fold greater than that of the neat

**Table 1**
Contact angle ($\theta$), nonpolar component ($\gamma_s^d$), polar component ($\gamma_s^p$) and surface energy ($\gamma_s$) values of unmodified (CN) and acetylated cellulose nanocrystals (ACNs).

| Sample | Contact angle $\theta$ (°) | | | $\gamma_s^d$ (mJ/m$^2$) | $\gamma_s^p$ (mJ/m$^2$) | $\gamma_s$ (mJ/m$^2$) |
|---|---|---|---|---|---|---|
| | Water | Diiodomethane | Ethylene glycol | | | |
| CN | 36.3 | 32 | 16.8 | 33.6 | 29.5 | 63.1 |
| ACN | 60.7 | 30 | 27.7 | 37.9 | 12.7 | 50.6 |

The surface tensions of three standard liquids were taken from the literature (Lin et al., 2011; Ly EhB et al., 2010) and are as follows: the $\gamma_L$, $\gamma_L^d$ and $\gamma_L^p$ values of water are 72.8, 21.8 and 51.0 mJ/m$^2$, respectively; the $\gamma_L$, $\gamma_L^d$ and $\gamma_L^p$ values of diiodomethane are 50.8, 49.5 and 1.3 mJ/m$^2$, respectively; and the $\gamma_L$, $\gamma_L^d$ and $\gamma_L^p$ values of ethylene glycol are 48.0, 29.0 and 19.0 mJ/m$^2$, respectively.

PU/ACN-0 film (0.98 MPa). Meanwhile, the $\varepsilon_b$ of the nanocomposites increased with the ACN content up to 10 wt%, and decreased after that. In this case, the $\varepsilon_b$ of the PU/ACN-10 film reached a maximum value of 444%, compared with a value of 208% for the neat PU film. The incorporation of ACN resulted in the separation between hard-segments and soft-segments in the PU matrix. The uniform dispersion of the ACN nanophase and the physical interaction between the ACN nanofiller and the PU matrix led to the enhancement of mechanical properties of the nanocomposite. This mechanical reinforcement was attributed to the formation of a rigid network by the cellulose nanocrystals in the host polymer matrix, which was governed by a percolation mechanism. In this mechanism the network is expected to form above the critical volume fraction at the percolation threshold, $V_{Rc}$, which depends on the aspect ratio ($L/d$) of the filler. In our case, the aspect ratio of ACN from cotton was about 13, leading to a $V_{Rc}$ value of ca. 5.4 vol%, i.e., 8.5 wt%. When excess nanofiller was added, such as in PU/ACN-10, PU/ACN-15, PU/ACN-20 and PU/ACN-25, a rigid network formed among the nanocrystals in the composites, which greatly facilitated the enhancement of strength and modulus; at the same time, the appearance of the rigid network and self-aggregation may have slightly damaged the original PU polymer structure (as seen by SEM) and blocked the movement of molecular chains. It is very unusual to improve the modulus while at the same time significantly improving the strength. These results indicate that ACN preferentially reinforced the hard microdomains rather than the soft segments of PU, avoiding the undesired stiffening of the soft domain, and thus maintained the large elongation at break of the polyurethane composites.

### 3.3. Fracture morphologies of PU/ACN nanocomposites

Fig. 3 shows the SEM images of the fracture morphologies of PU/ACN nanocomposites. The neat PU/ACN-0 film presented a smooth and striated fracture surface. When the ACN loading level was lower, such as 10 wt% (Fig. 3C), the modified nanocrystals dispersed homogeneously in the PU matrix, which was in good agreement with the results from the TEM image of PU/ACN-10 (Fig. 3G). This was an indication of a reasonable level of miscibility between PU and ACN. However, when the ACN loading level reached the $V_{Rc}$ or higher, nanoparticles began to self-aggregate and rigidity increased gradually, so the composites were relatively brittle and $\varepsilon_b$ decreased. When the ACN loading level continued to increase, nanoparticle self-aggregation and the density of the rigid

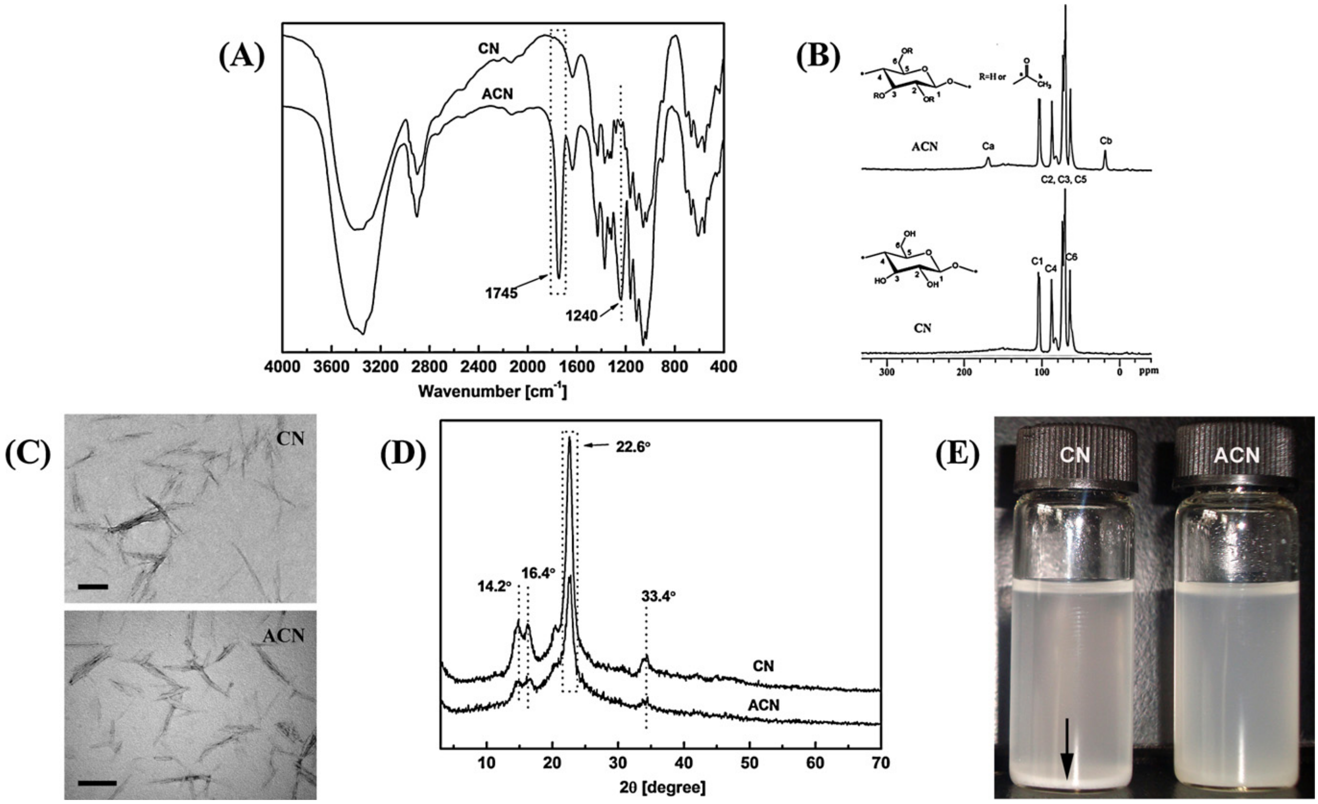

**Fig. 1.** FTIR spectra (A), $^{13}$C CP-MAS NMR spectra (B), TEM images (C), XRD patterns (D) and dispersibility observation in tetrahydrofuran (E) of unmodified CN and ACN (the scale is 200 nm in the TEM images, and the dispersibility observation was depicted for the CN in the left photograph and the CAN in the right photograph).

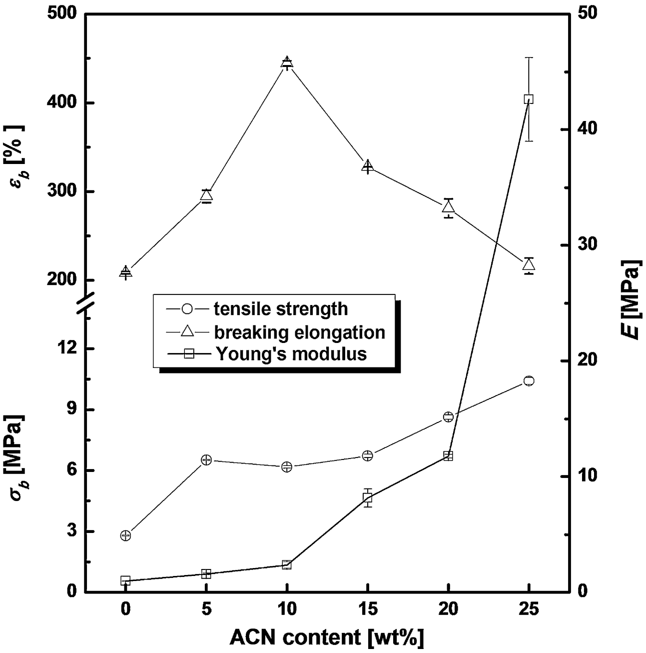

**Fig. 2.** Effect of ACN content on the $\sigma_b$, $\varepsilon_b$, and $E$ of PU/ACN nanocomposites as well as the PU/ACN-0.

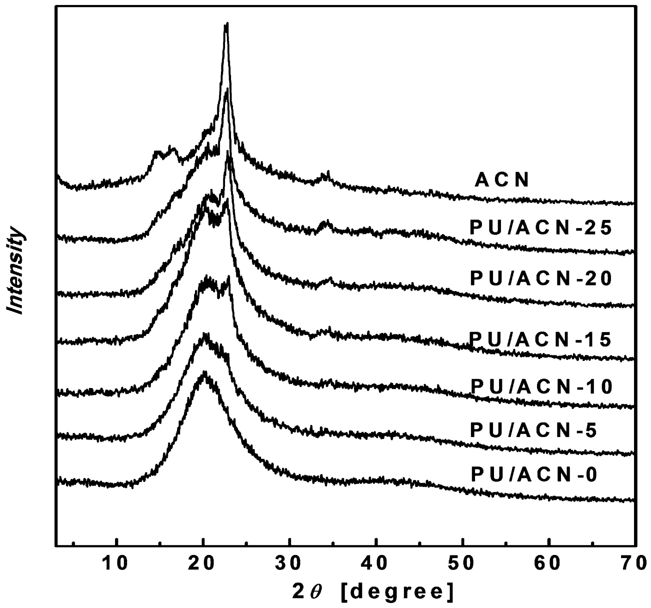

**Fig. 4.** XRD patterns of the PU/ACN nanocomposites as well as the polyurethane reference (PU/ACN-0) and the freeze-dried ACN powder.

parts increased simultaneously, damaging the inner structure of the matrix. The $\varepsilon_b$ then dropped further and the cross sections of the nanocomposites were more uneven (Fig. 3E and F).

### 3.4. Crystalline character of PU/ACN nanocomposites

The X-ray diffraction (XRD) spectra of pure PU and the PU/ACN nanocomposites are presented in Fig. 4. The $2\theta$ angles at 22.6° and 34.4° correspond to the typical reflection planes of cellulose I, 002 and 040 (Liu et al., 2010), respectively. Because of the low ACN content, the obvious peaks assigned to cellulose I were invisible in PU/ACN-1 and PU/ACN-5. With an increase in loading level the crystalline property of ACN exhibited two distinct diffraction peaks located at about 22.6° and 34.4°. These peaks indicate that the original crystal structure of cellulose I was well preserved in the nanocomposites. In particular, when more ACN was introduced (PU/ACN-20 and PU/ACN-25), the presence of ACN and even self-aggregated ACN, made the crystalline character assigned to the cellulose nanocrystals in the nanocomposite system more clear and definite.

### 3.5. Hydrogen bonding in PU/ACN nanocomposites

Fourier transform infrared (FTIR) spectra of pure PU and the PU/ACN nanocomposites are shown in Fig. 5A. As is well known, the hydrogen bond is an essential physical interaction in polyurethane affecting the microphase separation structure and mechanical properties of materials (Chen et al., 2008). In this case, the —NH

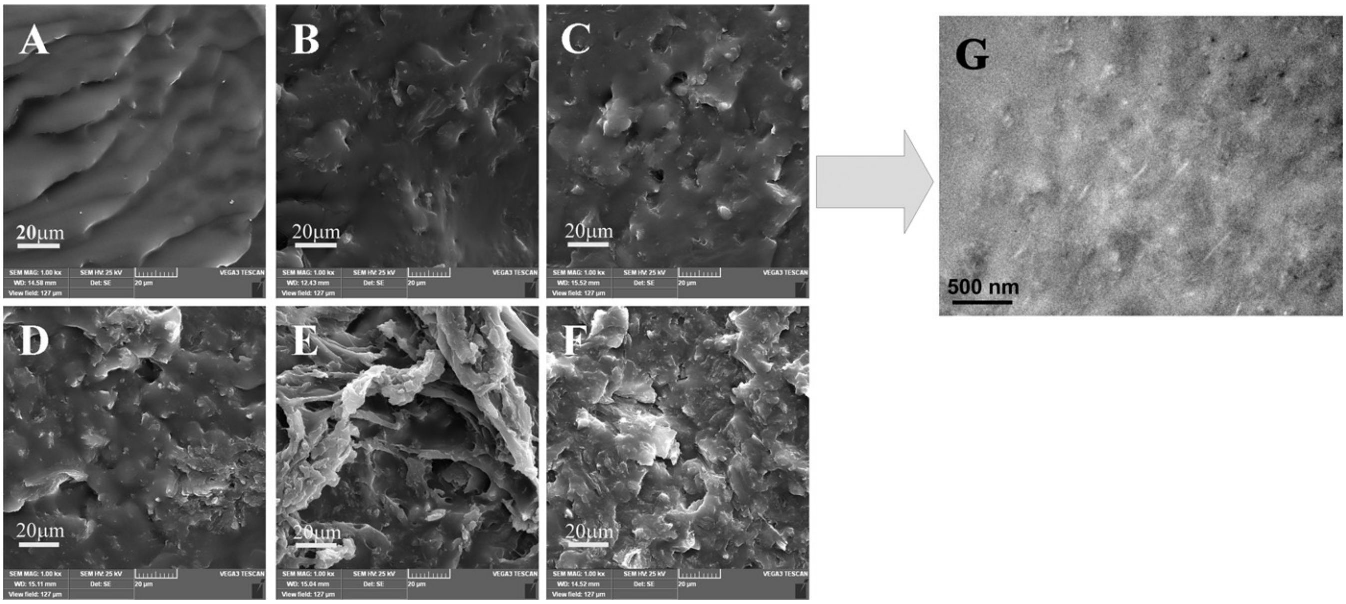

**Fig. 3.** SEM images of the fracture surfaces of the nanocomposites PU/ACN-5 (B), PU/ACN-10 (C), PU/ACN-15 (D), PU/ACN-20 (E), PU/ACN-25 (F) as well as PU/ACN-0 (A) for reference (the scale in each image is 20 μm), and the TEM image of ultrathin sections of polyurethane nanocomposite containing 10 wt% ACN (PU/ACN-10) (G).

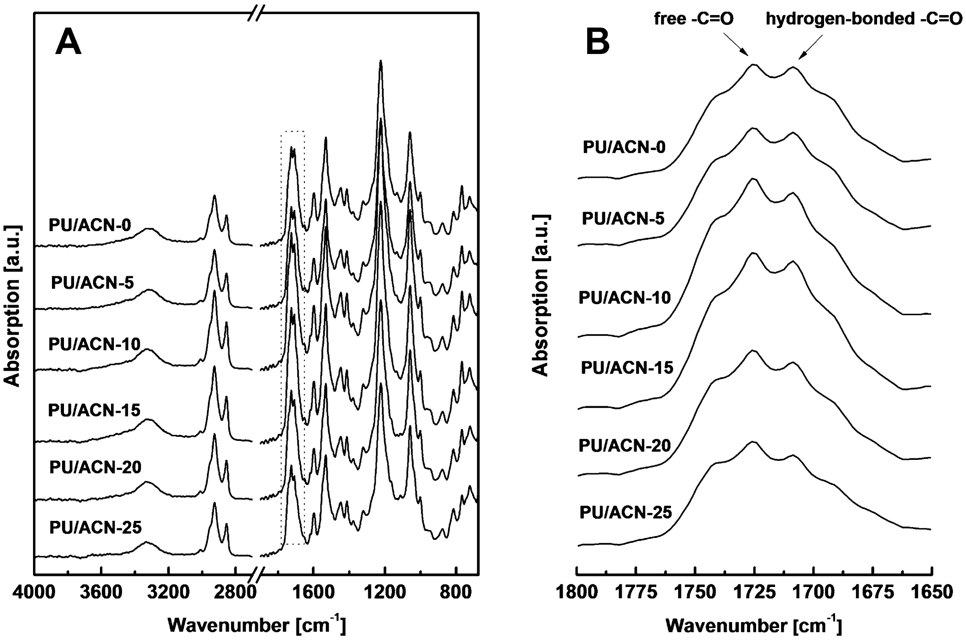

**Fig. 5.** FTIR spectra of PU/ACN nanocomposites with various ACN contents and the neat polyurethane (PC/ACN-0) (A), and FTIR spectra of PU/ACN nanocomposites and the neat polyurethane (PC/ACN-0) in the range of 1650–1800 cm$^{-1}$ (B).

in the hard-segment was hydrogen bonded with the —C=O of the hard-segment, the —C=O and —O— of the castor oil soft-segment, and the —C=O on the ACN surface after introducing ACN. In addition, —OH on the ACN surface that was not acetylated participated in hydrogen bonding with the —C=O in the soft- and hard-segments and —O— in the soft-segment. The carbonyl absorption band splits into two peaks, at 1707–1709 cm$^{-1}$ and 1736–1737 cm$^{-1}$, corresponding to hydrogen-bonded and free carbonyl groups, respectively, as shown in Fig. 5B. The carbonyl hydrogen-bonding index (Tien & Wei, 2001), i.e., the intensity ratio of the free carbonyl peak to the hydrogen-bonded carbonyl peak, increased with an increase in the ACN loading level. It suggested that hydrogen bonding associated with carbonyl groups in hard- and soft-segments in PU was partially inhibited due to the introduction of ACN, in spite that the rigid rod-like cellulose nanocrystals were hydrogen bonded with the polyurethane molecular chains. Moreover, this gave the molecular chains in amorphous region more freedom of motion, and led to a lower glass transition temperature ($T_g$), which was in good agreement with the DSC and DMA results.

### 3.6. Thermal properties of PU/ACN nanocomposites

In the PU/ACN nanocomposites, the glass transition temperature ($T_g$) of the castor oil soft-segment can be affected by ACN in two opposite ways. First, the motion of the soft-segment may be suppressed by the steric hindrance of the rigid ACN nanophase and by hydrogen bonding onto the active ACN surface. This could result in a shift of $T_g$ to a higher temperature. In the opposite way, incorporating ACN may cleave the original interaction between the hard- and soft-segments. This influence of ACN on the phase separation structure at domain scale would lead to a decrease in the glass transition temperature ($T_g$) of polyurethane. Especially at molecular level, the soft-segment could escape the binding of the hard-segment, leading to decreased $T_g$. DSC data for the glass transition temperature at midpoint ($T_{g,\,mid}$) and heat-capacity increment ($\Delta C_p$) of the nanocomposites as well as the normalized heat-capacity increment of the PU matrix ($\Delta C_{p,\,PU}$) are summarized in Table 2. All PU/ACN nanocomposites showed lower $T_{g,\,mid}$ values than that of neat PU. It suggested that the inevitable cleavage of the original interaction between the hard- and soft-segments and the effect of the resulted organization structure of all components in the nanocomposite were dominant, in spite of ACN restricting the mobility of soft-segments and relative to the formation of new hydrogen bonds. Thus, the hydrogen bonding associated with carbonyl groups in hard- and soft-segments was destroyed in the PU matrix, which was in agreement with the increasing fraction of free carbonyl compared to the hydrogen-bonded carbonyl shown by the FTIR analysis. Usually, the $\Delta C_p$ decreases with a decrease of $T_{g,\,mid}$. However, in this case, the $\Delta C_{p,\,PU}$ values of most PU/ACN nanocomposites were equivalent to and even slightly higher than that of neat PU except for the slightly low $\Delta C_{p,\,PU}$ of the PU/ACN-5 containing the lowest loading-level of ACN. It indicated that the intensity of interaction at molecular level between soft-segment and other components in the nanocomposite system of PU/ACN was analogical to that between soft-segment and hard-segment in neat PU.

Dynamic mechanical analysis (DMA) allows determination of the mechanical behavior of materials over a broad temperature range and is strongly sensitive to the morphology and structure of the composite. A spectacular improvement in the storage modulus was achieved by introducing ACN into the PU matrix, as shown in Fig. 6A. Below $T_g$, the moduli of the nanocomposites were slightly higher than that of the neat PU matrix; however, there was a significant reinforcement effect in the low modulus region above $T_g$. The modulus of the nanocomposites containing 25 wt% ACN was more than 14 times that of the pure PU at 70 °C. This reinforcement is due to both cellulose nanocrystal reinforcement and increased effective cross-link density of the rubber network from the PU-ACN interaction. For the neat PU and lower concentration nanocomposites the modulus (Fig. 6A) showed a sharp decrease during the glass-rubber transition and kept decreasing with temperature in the rubbery region due to the thermoplastic nature of the material. For higher concentration nanocomposites, the drop in storage modulus was dramatically reduced as the PU combined and covalently linked with ACN.

**Table 2**
DSC and DMA data for PU/ACN nanocomposites as well as the neat polyurethane (PU/ACN-0).

| Sample | DSC data | | | DMA data | | | |
|---|---|---|---|---|---|---|---|
| | $T_{g,mid}$ (°C) | $\Delta C_p$ (J/g K) | $\Delta C_{p,PU}$ (J/g K) | $T_{\alpha,onset}$ (°C) | $E'$ ($\times 10^3$ MPa) | $T_{\alpha\ max}$ (°C) | tan $\delta$ |
| PU/ACN-0 | 14.5 | 0.60 | 0.60 | 0.8 | 1.42 | 28.0 | 1.34 |
| PU/ACN-5 | 7.2 | 0.49 | 0.52 | −0.1 | 1.94 | 22.9 | 1.15 |
| PU/ACN-10 | 7.7 | 0.57 | 0.63 | −7.2 | 2.06 | 20.3 | 0.90 |
| PU/ACN-15 | 7.1 | 0.49 | 0.58 | −7.8 | 2.12 | 20.0 | 0.77 |
| PU/ACN-20 | 7.1 | 0.61 | 0.76 | −9.4 | 2.35 | 19.6 | 0.81 |
| PU/ACN-25 | 4.9 | 0.47 | 0.63 | −9.2 | 2.06 | 20.8 | 0.61 |

The significant mechanical reinforcement observed in the PU/ACN nanocomposites above $T_g$ suggests the formation of rigid particle networks by the cellulose nanocrystals in the host polymer matrix, where stress transfer is facilitated by hydrogen-bonding between the nanocrystals, governed by the percolation mechanism which has been discussed above. Notably, the PU/ACN nanocomposite with the highest elongation at break was obtained with 10 wt% ACN, while Young's modulus and tensile strength continued to increase. Thus, we can conclude that with the formation of a cellulose network, the modulus and strength of the nanocomposites increased as the ACN content increased. On the other hand, rigid particle networks resulted in a decrease in elongation at break, as characterized by mechanical tests.

Thermodynamic incompatibility resulting from phase separation between the soft- and hard-segments of PU plays a key role in the physical properties. The influence of ACN on the phase separation structure was demonstrated by the decrease in the glass transition temperature ($T_g$) of polyurethane. The dependence of tan

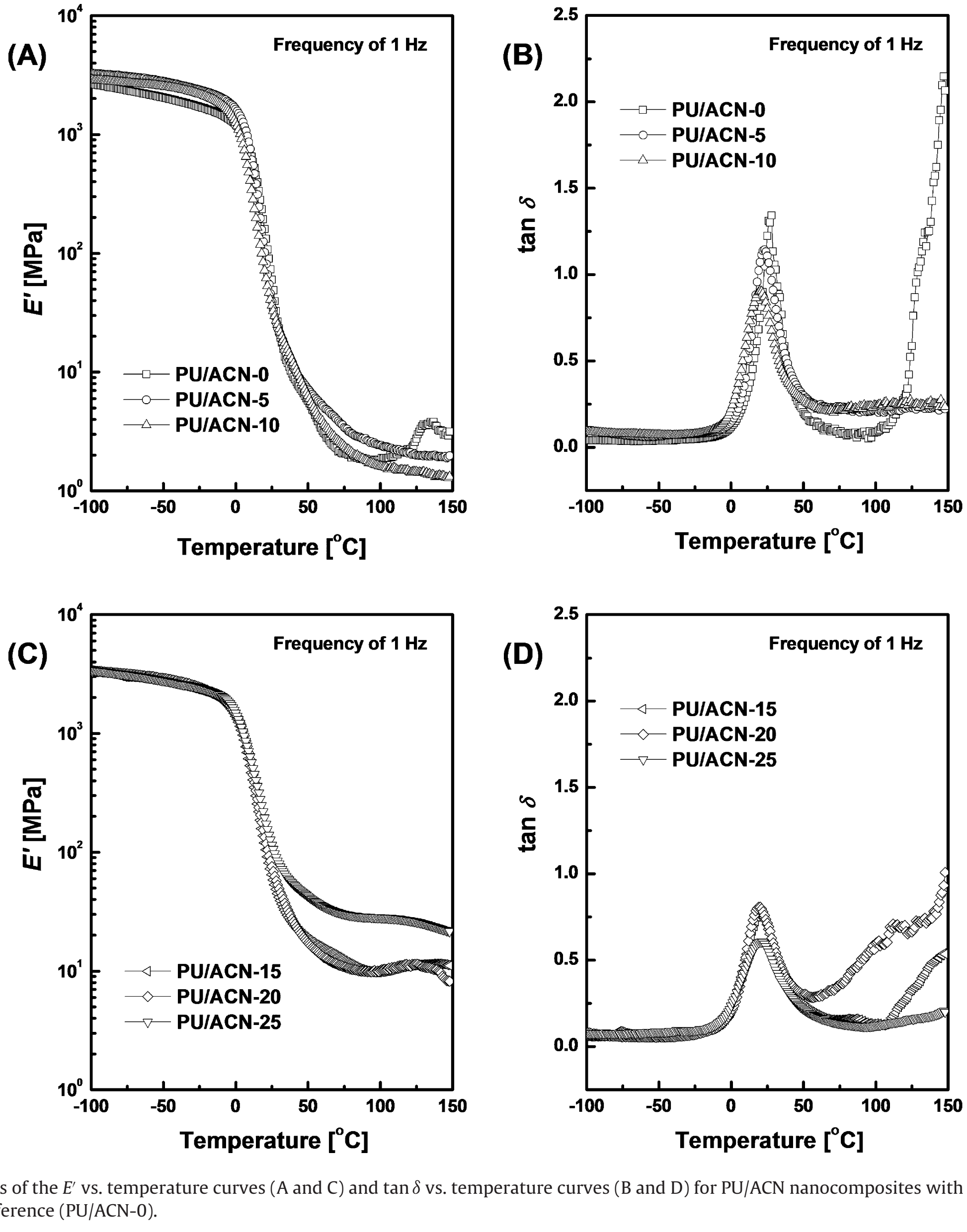

**Fig. 6.** DMA thermograms of the $E'$ vs. temperature curves (A and C) and tan $\delta$ vs. temperature curves (B and D) for PU/ACN nanocomposites with various ACN contents and the neat polyurethane reference (PU/ACN-0).

$\delta$ on temperature for PU and PU/ACN nanocomposites is shown in Fig. 6B. The α-relaxation temperatures of the amorphous soft segment domains, i.e. the $T_{\alpha\ \max}$ of PU soft segments were 28.0, 22.9, 20.3, 20.0, 19.6 and 20.8 °C, for neat PU, PU/ACN-5, PU/ACN-10, PU/ACN-15, PU/ACN-20 and PU/ACN-25, respectively. The decrease in $T_{\alpha\ \max}$ for the nanocomposites was due to the fact that ACN associated strongly with the hard segment of PU, resulting in a lower fraction of hydrogen bonded carbonyl groups in the hard segment and an increase in the degree of freedom for the PU soft segment. These results were consistent with FTIR results. The sharpness and height of the damping peaks give information about the degree of order and the freedom of motion of the molecules in the soft domains (Tsagaropoulos & Eisenberg, 1995; Son, Lee, & Lim, 1999). This may be attributed to the greatly restricted motion of PU chains resulting from hydrogen bonding and cross-linking between PU molecules and nanoscale ACN, as indicated by FTIR.

## 4. Conclusions

We have demonstrated the synthesis of polyurethane nanocomposites with high tensile strength and elongation at break and greatly improved modulus using very high amounts of acetylated cellulose nanocrystals (a biobased material) as the reinforcing filler and castor oil as the soft-segment. The cellulose nanocrystal was modified by the substitution of hydroxyl groups on the CN surface with acetyl groups, while its crystalline structure remained intact. Acetylated cellulose nanocrystals exhibited improved dispersion in polar solvents and a decrease in surface polarity. The tensile strength and Young's modulus of the nanocomposites were enhanced from 2.79 MPa to 10.41 MPa and from 0.98 MPa to 42.61 MPa, respectively, when the ACN content was increased to a surprising 25 wt%. These materials display a significant mechanical reinforcement, especially above $T_g$. This effect is well-described by the microphase separation and percolation model, and is indicative of the formation of a percolating particle network in which stress transfer is facilitated by hydrogen-bonding between the particles. The results of this study will have a great impact on broadening the practical use and applications of high biomass-based polymer nanocomposite materials.

## Acknowledgements

The research work was financially supported by the Program of New Century Excellent Talents, Ministry of Education of China (NCET-11-0686); Fundamental Research Funds for the Central Universities (Self-Determined and Innovative Research Funds of WUT 2012-Ia-006); ecoENERGY Innovation Initiative of Canada; and Program of Energy Research and Development (PERD) of Canada.

## Appendix A. Supplementary data

Supplementary data associated with this article can be found, in the online version, at http://dx.doi.org/10.1016/j.carbpol.2013.02.023.

## References

Anglès, M. N., & Dufresne, A. (2000). Plasticized starch/tunicin whiskers nanocomposites. 1. Structural analysis. *Macromolecules*, *33*, 8344–8353.

Attala, R. H., Gast, J. C., Sindorf, D. W., Bartuska, V. J., & Maciel, G. E. (1980). *Journal of American Chemistry Society*, *102*, 3249–3251.

Azizi Samir, M. A. S., Alloin, F., Sanchez, J. Y., & Dufresne, A. (2004). Cellulose nanocrystals reinforced poly(oxyethylene). *Polymer*, *45*, 4149–4157.

Azizi Samir, M. A. S., Alloin, F., Sanchez, J. Y., El Kissi, N., & Dufresne, A. (2004). Preparation of cellulose whiskers reinforced nanocomposites from an organic medium suspension. *Macromolecules*, *37*, 1386–1393.

Buschle-Diller, G., & Zeronian, S. H. (1992). Enhancing the reactivity and strength of cotton fibers. *Journal of Applied Polymer Science*, *45*, 967–979.

Cao, X., Dong, H., & Li, C. M. (2007). New nanocomposite materials reinforced with flax cellulose nanocrystals in waterborne polyurethane. *Biomacromolecules*, *8*, 899–904.

Cao, X., Habibi, Y., & Lucia, L. A. (2009). One-pot polymerization, surface grafting, and processing of waterborne polyurethane–cellulose nanocrystal nanocomposites. *Journal of Material Chemistry*, *19*, 7137–7145.

Capadona, J. R., van den Berg, O., Capadona, L. A., Schroeter, M., Rowan, S. J., Tyler, D. J., et al. (2007). A versatile approach for the processing of polymer nanocomposites with self-assembled nanofibre templates. *Nature Nanotechnology*, *2*, 765–769.

Capadona, J. R., Shanmuganathan, K., Tyler, D. J., Rowan, S. J., & Weder, C. (2008). Stimuli-responsive polymer nanocomposites inspired by the sea cucumber dermis. *Science*, *319*, 1370–1374.

Chazeau, L., Cavaillé, J. Y., Canova, G., Dendievel, R., & Boutherin, B. (1999). Viscoelastic properties of plasticized PVC reinforced with cellulose whiskers. *Journal of Applied Polymer Science*, *71*, 1797–1808.

Chen, G., Wei, M., Chen, J. H., Huang, J., Dufresne, A., & Chang, P. R. (2008). Simultaneous reinforcing and toughening: New nanocomposites of waterborne polyurethane filled with low loading level of starch nanocrystals. *Polymer*, *49*, 1860–1870.

Dubief, D., Samain, E., & Dufresne, A. (1999). Polysaccharide microcrystals reinforced amorphous poly(b-hydroxyoctanoate) nanocomposite materials. *Macromolecules*, *32*, 5765–5771.

Dufresne, A. (2008). Polysaccharide nano crystal reinforced nanocomposites. *Canadian Journal of Chemistry*, *86*, 484–494.

Fabbri, P., Champon, G., Castellano, M., Belgacem, M. N., & Gandini, A. (2004). Reactions of cellulose and wood superficial hydroxy groups with organometallic compounds. *Polymer International*, *53*, 7–11.

Favier, V., Chanzy, H., & Cavaillé, J. Y. (1995). Polymer nanocomposites reinforced by cellulose whiskers. *Macromolecules*, *28*, 6365–6367.

Gao, Z., Peng, J., Zhong, T., Sun, J., Wang, X., & Yue, C. (2012). Biocompatible elastomer of waterborne polyurethane based on castor oil and polyethylene glycol with cellulose nanocrystals. *Carbohydrate Polymers*, *87*, 2068–2075.

Habibi, Y., Lucia, L. A., & Rojas, O. J. (2010). Cellulose nanocrystals: Chemistry, self-assembly, and applications. *Chemical Reviews*, *110*, 3479–3500.

Hussain, F., Hojjati, M., Okamoto, M., & Gorga, R. E. (2006). Review article: Polymer–matrix nanocomposites, processing, manufacturing, and application: An overview. *Journal of Composite Materials*, *40*, 1511–1575.

Lin, N., Chen, G., Huang, J., Dufresne, A., & Chang, P. R. (2009). Effects of polymer-grafted natural nanocrystals on the structure and mechanical properties of poly(lactic acid): A case of cellulose whisker-graft-polycaprolactone. *Journal of Applied Polymer Science*, *113*, 3417–3425.

Lin, N., Huang, J., Chang, P. R., Feng, J., & Yu, J. (2011). Surface acetylation of cellulose nanocrystal and its reinforcing function in poly(lactic acid). *Carbohydrate Polymers*, *83*, 1834–1842.

Liu, H., Liu, D., Yao, F., & Wu, Q. (2010). Fabrication and properties of transparent polymethylmethacrylate/cellulose nanocrystals composites. *Bioresource Technology*, *101*, 5685–5692.

Ljungberg, N., Bonini, C., Bortolussi, F., Boisson, C., Heux, L., & Cavaillé, J. Y. (2005). New nanocomposite materials reinforced with cellulose whiskers in atactic polypropylene: Effect of surface and dispersion characteristics. *Biomacromolecules*, *6*, 2732–2739.

Ly EhB, Bras, J., Sadocco, P., Belgacem, M. N., Dufresne, A., & Thielemans, W. (2010). Surface functionalization of cellulose by grafting oligoether chains. *Materials Chemistry and Physics*, *120*, 438–445.

Morin, A., & Dufresne, A. (2002). Nanocomposites of chitin whiskers from Riftia tubes and poly(caprolactone). *Macromolecules*, *35*, 2190–2199.

Owens, D. K., & Wendt, R. C. (1969). Estimation of the surface free 635 energy of polymer. *Journal of Applied Polymer Science*, *13*, 1741–1747.

Pei, A., Malho, J. M., Ruokolainen, J., Zhou, Q., & Berglund, L. A. (2011). Strong nanocomposite reinforcement effects in polyurethane elastomer with low volume fraction of cellulose nanocrystals. *Macromolecules*, *44*, 4422–4427.

Schroers, M., Kokil, A., & Weder, C. (2004). Solid polymer electrolytes based on nanocomposites of ethylene oxide–epichlorohydrin copolymers and cellulose whiskers. *Journal of Applied Polymer Science*, *93*, 2883–2888.

Shanmuganathan, K., Capadona, J. R., Rowan, S. J., & Weder, C. (2010a). Bio-inspired mechanically-adaptive nanocomposites derived from cotton cellulose whiskers. *Journal of Material Chemistry*, *20*, 180–186.

Shanmuganathan, K., Capadona, J. R., Rowan, S. J., & Weder, C. (2010b). Stimuli-responsive mechanically adaptive polymer nanocomposites. *ACS Applied Material and Interfaces*, *2*, 165–174.

Shopsowitz, K. E., Qi, H., Hamad, W. Y., & MacLachlan, M. J. (2010). Free-standing mesoporous silica films with tunable chiral nematic structures. *Nature*, *468*, 422–425.

Son, T. W., Lee, D. W., & Lim, S. K. (1999). Thermal and phase behavior of polyurethane based on chain extender, 2,2-bis-[4-(2-hydroxyethoxy)phenyl]propane. *Polymer Journal*, *31*, 563–568.

Sperling, L. H., & Manson, J. A. (1983). Interpenetrating polymer networks from trilyceride oils containing special functional groups: A brief review. *Journal of American Oil Chemists Society*, *60*, 1887–1892.

Tien, Y. I., & Wei, K. H. (2001). Hydrogen bonding and mechanical properties in segmented montmorillonite/polyurethane nanocomposites of different hard segment ratios. *Polymer*, *42*, 3213–3221.

Tjong, S. C. (2006). Structural and mechanical properties of polymer nanocomposites. *Materials Science and Engineering R-Reports*, *53*, 73–197.

Tsagaropoulos, G., & Eisenberg, A. (1995). Dynamic mechanical study of the factors affecting the two glass transition behavior of filled polymers. Similarities and differences with random ionomers. *Macromolecules*, *28*, 6067–6077.

Wu, Q., Henriksson, M., Liu, X., & Berglund, L. A. (2007). A high strength nanocomposite based on microcrystalline cellulose and polyurethane. *Biomacromolecules*, *8*, 3687–3692.